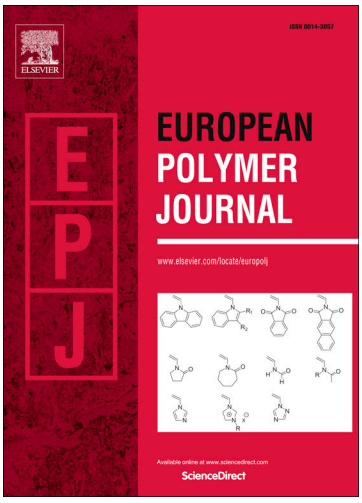

Magnetic nanocomposites based on shape memory polyurethanes

G.D. Soto, C. Meiorin, D. Actis, P. Mendoza Zélis, Oscar Moscoso Londoño, Diego Muraca, M.A. Mosiewicki, N.E. Marcovich

PII: S0014-3057(18)31062-0
DOI: https://doi.org/10.1016/j.eurpolymj.2018.08.046
Reference: EPJ 8559

To appear in: *European Polymer Journal*

Received Date: 11 June 2018
Revised Date: 9 August 2018
Accepted Date: 27 August 2018

Please cite this article as: Soto, G.D., Meiorin, C., Actis, D., Mendoza Zélis, P., Londoño, O.M., Muraca, D., Mosiewicki, M.A., Marcovich, N.E., Magnetic nanocomposites based on shape memory polyurethanes, *European Polymer Journal* (2018), doi: https://doi.org/10.1016/j.eurpolymj.2018.08.046

MAGNETIC NANOCOMPOSITES BASED ON SHAPE MEMORY POLYURETHANES

G. D. Soto[1], C. Meiorin[1], D. Actis[2], P. Mendoza Zélis[2], Oscar Moscoso Londoño[3], Diego Muraca[3], M. A. Mosiewicki[1], N. E. Marcovich[1]*

[1] Instituto de Investigaciones en Ciencia y Tecnología de Materiales (INTEMA-CONICET)

Juan B. Justo 4302, Mar del Plata, Buenos Aires, Argentina; CP 7600

[2] Instituto de Física La Plata (CONICET), Universidad Nacional de La Plata;

Calle 49 y 115, La Plata, Buenos Aires, Argentina; CP 1900

[3] Instituto de Física Gleb Wataghin (IFGW), Universidade Estadual de Campinas – UNICAMP, Campinas, São Paulo, Brazil

ABSTRACT

Shape-memory composites based on a commercial segmented polyurethane and magnetite (Fe_3O_4) nanoparticles (MNPs) were prepared by a simple suspension casting method. The average sizes of individual magnetic particles/clusters were determined by TEM microscopy and corroborated from SAXS patterns. The magnetization properties of selected samples were evaluated using zero field cooling/field cooling (ZFC/FC) measurements and magnetization loops obtained at different temperatures. The results showed that magnetization at high field (20 kOe) and coercitivity measured at 5 K increase with magnetite content and that all the composite films exhibit super-paramagnetic behavior at 300 K. The specific absorption rate (SAR) of the nanocomposites was calculated by experimentally determining both the specific heat capacity and the heating rate of the films exposed to an alternant magnetic field. All nanocomposites were able to increase their temperature when exposed to an alternant magnetic field, although the final temperature reached resulted dependent of the MNPs concentration. What is more, a fast and almost complete recovery of the original shape of the nanocomposites containing more than 3 nominal wt.% MNP was obtained by this remote activation applied to the previously deformed samples.

KEYWORDS: Polymeric nanocomposites; Shape memory properties; Magnetic heating; indirect triggering method.

INTRODUCTION

In recent years shape memory polymers (SMPs) have found growing interests because of their special and unique applications in medical, electronics, hightech industries as well as daily life [1, 2]. SMPs are found to be a superior choice for developing novel intelligent polymers due to their low density, economic cost, processability, appreciable shape recovery properties [1, 2], high repeated deformation and possibility to modify the material by introducing fillers [3, 4]; moreover, their properties can be fine-tuned to requirements via changes in materials additives and synthesis methods [3]. These smart polymers can be programmed so as to change their original permanent shape into a secondary temporary shape through exposing them to external stimuli such as temperature, light, chemicals, pH, magnetic field, etc. [4-6]. Among these polymers, thermoplastic segmented polyurethanes (TPU) pose shape-memory property activated by heating and also have excellent chemical stability, potential biocompatibility and biodegradability [7]. However, sometimes direct heating is not feasible and thus other methods such as inductive remote heating have to be considered [2, 5]. One interesting method is the use of magnetic nanoparticles within polymer matrix to achieve fast and remote response when exposed to an alternant magnetic field [3, 5, 7].

Thermomagnetic or electromagnetic shape memory effect in nanocomposites can be reached by adding particles of metal or their oxides [3] as fillers (i.e. iron oxide, neodymium magnet particles, nickel powder or ferromagnetic particles) into a TPU. Magnetic properties are introduced to polymer composites usually by using micro or nano-sized ZnNi or Fe_3O_4 particles [3].

The synthesis of magnetite nanoparticles (NPs) with controlled size has been extensively studied for years because of the potential applications in biomedicine and other relevant areas due to their favorable magnetic properties, low toxicity, high chemical stability and biocompatibility [2, 8-10]. Fe_3O_4 particles have been found to be suitable for in vivo use and have been widely investigated for applications such as magnetic resonance imaging contrast agents and hyperthermia procedures for cancer treatments [2]. However, the incorporation of NPs on different polymeric matrices is a relatively new area of study [11]. Different strategies were developed to disperse NPs within the matrix in order to avoid oxidation and agglomeration, mainly coating with organic shells, including surfactants and polymers and either with inorganic components

[12]. At the same time, single-domain magnetic NPs can be exploited to activate the shape memory property upon the application of an alternant magnetic field due to their capacity to transfer energy from the radio frequency [13] field to the medium via heat dissipation. The magnetic Fe_3O_4 particles with sub-100 nm dimension can be used as inductive heaters in SMPs [2, 5]. The impact of particle size on the energy loss and heating mechanism is complicated, but well described [3, 14]. The induction mechanism can be described by the Néel-Brown relaxation model for single-domain ferromagnetic particles [3, 13, 15]. Usually this model consider non-interacting single-domain nanoparticles and low field; nevertheless the model can be extended to system with the presence of dipolar interaction [15, 16]. In the material, magnetic domains can be simplified considering a net magnetization vector. This will follow any applied external magnetic field. In an alternant magnetic field (with relative high frequency), the magnetic vector cannot follow the magnetic field change rate, being out of phase with the magnetic field, which generates magnetic energy dissipation that is transformed into thermal energy. Such losses are described by the Néel-Brown model. The Néel relaxation involves coherent change orientation of the magnetic moments and not the physical volume rotation of the particle, while, in Brown relaxation, the magnetic moments are locked with the particle axis and the whole particle rotates [3, 17]. The time of relaxation depends on the particle diameter, but also on the material considered: for magnetite particles below 10 nm, the fast Néel relaxation dominates, while larger particles tend to follow the Brown model [18]. Thus, the obtaining of magnetic composites with exceptional shape memory properties requires a strict control of the size of the magnetic particles but also a uniform dispersion of them into the polymeric matrix.

As reported in our previous work [4], the incorporation of magnetite nanoparticles to a commercial TPU did not significantly affect most of the matrix properties, including its shape memory behavior, while added magnetic response to the nanocomposites. Moreover, the composite containing 10 nominal wt.% of magnetic particles had fast magnetic responsiveness. However, the effect of nanoparticle concentration on the magnetic response and inductive heating was not fully investigated and thus it is reported in the present paper.

MATERIALS AND METHODS

Preparation of nanocomposites: samples were prepared by casting and drying of suspensions obtained by dispersing the synthesized magnetic nanoparticles (MNP) into the dimethylformamide solution of the segmented polyurethane (IROGRAN PS455-203, Huntsman). The procedure was presented in detail in a previous paper [4] and thus is only summarized here. In brief, to prepare the magnetic nanoparticles, 0.09 mol of $FeCl_3 \cdot 6H_2O$ and 0.06 mol of $FeCl_2.4H_2O$ were poured into a flask containing 50 mL of distilled water and heated at 70 °C to dissolve the salts. Then, 40 mL of NH_4OH were added and the formation of a black precipitate was immediately observed. With the help of a super-magnet positioned out of the flask, the MNPs were decanted and collected into centrifugation tubes and washed until neutral pH with distilled water, separating the water used in each wash by centrifugation. Finally, the MNPs were placed in a Petri dish and lyophilized. The obtained dark thin powder was preserved in a reagent bottle.

To prepare the composite films, polyurethane pellets were dissolved in dimethylformamide (DMF) up to 20 wt.% at room temperature by using a magnetic stirrer, and then mixed with the previously synthesized MNPs in suitable ratios to obtain composite samples. The mixture was then ultrasonicated for 6 h to obtain a stable and homogeneous suspension. Composite films (approximately 0.75 mm in thickness) were prepared by solvent casting of the final suspensions on a glass plate followed by drying in a convection oven at 80 °C for 24 hours.

The chosen nomenclature for the nanocomposites was PU-1, PU-3, PU-5, PU-7 and PU-10, for samples with 1, 3, 5, 7 and 10 nominal wt.% of MNP, respectively.

Transmission Electron Microscopy (TEM): The morphology and particle size of the synthesized nanoparticles were investigated by transmission electron microscopy. This study was performed on a TEM-FEG (JEM 2100F) field-emission gun transmission electron microscope (voltage: 200 kV, spot size 3). The images were acquired using a Gatan, Orius SC600/831 camera at different resolutions. Magnetite particles were dispersed in ultrapure water (resistivity = 18.2 MΩ·cm at 25 °C) and sonicated during 15 minutes. The samples for microscopy observation were prepared by drying a drop of the nanoparticle suspension during 24 hours at room temperature on a Ted Pella ultrathin cooper film on a holey carbon.

Static magnetic properties: The magnetic properties of the PU-magnetite composites were determined using a superconducting quantum interference device (SQUID)

magnetometer (Quantum Design, MPMS XL). The samples were characterized in terms of their isothermal magnetization curves by obtaining the specific magnetization (M) against the applied magnetic field (H) up 1600 kA/m (20 kOe) at different temperatures and also by performing the Zero Field Cooling/Field Cooling (ZFC/FC) measurements. The ZFC/FC measurement protocol was carried out as follows: the sample was first cooled down from 300 K to 5 K under a zero magnetic field, then a static field of 4 kA/m (50 Oe) was applied and the magnetization was measured while increasing the temperature up to 300 K (ZFC). Subsequently (FC mode), the sample was cooled down up to 5 K under the same applied magnetic field (4 kA/m) and the magnetization was measured while warming up the sample from 5 K to 300 K. Samples used for these tests were previously conditioned in a closed container with silica gel until they reached their equilibrium moisture content (about 5-7 wt.%).

Small-angle X-ray scattering (SAXS): SAXS patterns of the PU based composite films were obtained on the D1B-SAXS1 beamline at the Brazilian Synchrotron Light Laboratory (LNLS, Campinas, Brazil). The measurements were carried out at 20 and 60 ºC. All data were collected using a 300 k Pilatus bidimensional detector operating at a wavelength of k = 1.822 Å. The scattering intensity, I, was measured as function of momentum transfer vector q ($q = 4\pi \sin\theta/\lambda$), in a range from 0.1 to 5.0 nm^{-1}, being "θ" the scattering angle. To analyze the results, the matrix curve was subtracted from the SAXS patterns of the nanocomposites.

Determination of the specific heat capacity: The specific heat capacity of film samples was determined by the differential scanning calorimetry (DSC) technique according to the ASTM standard test method E 1269-01 based in a comparison with a sapphire standard. Samples of the composites (~0.7 mg) were analyzed in a calorimeter (Perkin Elmer Pyris 1) provided with a cooling unit, operating under dry nitrogen atmosphere (20 mL/min). Measurements were performed at a rate of 20 ºC/min from the initial temperature (-40 ºC) up to the final temperature (80 ºC).

Magnetic heating of composites: The heating response of rectangular nanocomposite samples of 3.5 mm x 5 mm exposed to an alternant magnetic field was characterized using an inductive heating equipment (a power source-resonator set Hüttinger TIG 2.5/300) at a frequency of 260 kHz and field amplitude of 48.5 kA/m. The sample temperature was measured by an optic fiber sensor (Neoptix T1), with an accuracy of 0.1 ºC, immersed in the center of the material and connected to an interface (Neoptix

Reflex). Measurements were performed in triplicate. Experimental Specific Absorption Rate (SAR) was determined from the slope of the heating curve (dT/dt) as follows:

$$SAR = \frac{dT}{dt} * \frac{Cp}{[\mathrm{MNP}]} \quad (1)$$

where Cp is the specific heat capacity of the sample (J (K kg composite film)$^{-1}$) and [MNP] is the mass fraction of magnetic nanoparticles (MNP) in the composite film. Also, images of temperature profiles at different times (0, 4, 8, 11, 18, 25, 33, 46 and 58 s) of multiple specimens submitted to an alternant magnetic field of 143 kHz and 18.9 ± 6 kA/m (samples located at the corner) or 17.8 ± 2 kA/m (other samples) were recorded with a thermographic camera TESTO 870-1 for illustrative purposes.

Shape memory behavior: The shape memory response of the composites to an external magnetic field was qualitatively evaluated. Rectangular strips of about 5 mm x 35 mm were first heated at 70 ℃ in an oven and then deformed. The deformed shape was fixed by decreasing suddenly sample temperature by applying a thermal fault locator spray, which ensures a rapid cooling until about -48 ℃ [4]. The samples were then submitted to a radiofrequency field (48.5 kA/m, 260 kHz), and the shape recovery was recorded with a video camera. These tests were performed in duplicate.

RESULTS AND DISCUSSION

Figure 1 shows some TEM images taken from a diluted particle suspension. The nanoparticles synthesized by the co-precipitation method [4] present different shapes, i.e. nearly spherical, nearly cubic, hexagonal shaped, etc. and are polydisperse, the size of the individual MNPs ranged from about 5–12 nm. Moreover, the images taken with high magnification also suggest that clusters with average diameters varying from 10 to 25 nm form when particles are dispersed in the solvent, due to surface energy minimization [19].

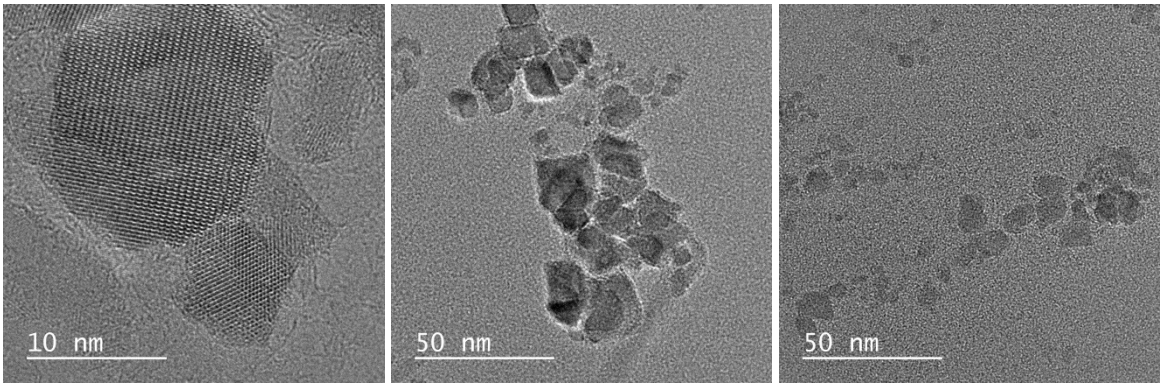

Figure 1: TEM micrographs of magnetic nanoparticles.

Figure 2 shows the temperature dependence of the magnetization in the ZFC and FC measurements for the PU-1, PU-7 and PU-10 samples. The general feature of the M vs. T curves is similar for the three samples. Irreversibility temperature (defined as the threshold temperature above which FC and ZFC curves coincide) is near room temperature and the ZFC-FC behavior shows a typical behavior of nanoparticle systems with a very wide energy distribution, $U=KV$ (where K is the magnetic anisotropy and V the magnetic volume of the magnetic entities, iron oxide nanoparticles in this case). Thus, the broadness of this energy distribution is due to both the wide size distribution (related to V) but also to shape anisotropy (related to K), as can be deduced from the different particle shapes and sizes observed by TEM. Also, dipolar interaction between the magnetic nanoparticles could affect this wide energy distribution. Anyhow, if the origin of the energy distribution came from the anisotropy volume product (KV) of the nanoparticle or from dipolar interactions, it does not show significant differences between samples containing different amounts of MNPs. To confirm this behavior, the temperature distribution and mean values of blocking temperatures were obtained from $\langle T_B \rangle$= d(ZFC-FC)/dT for the three samples and negligible differences between their $\langle T_B \rangle$ were obtained, as shown in Figure 3 and Table 1. Considering the sensitiveness of the measurement and that this value is directly related to the energy barrier (anisotropy plus dipolar) of the system, we can assume that the magnetic entities are very similar, independently of sample concentration.

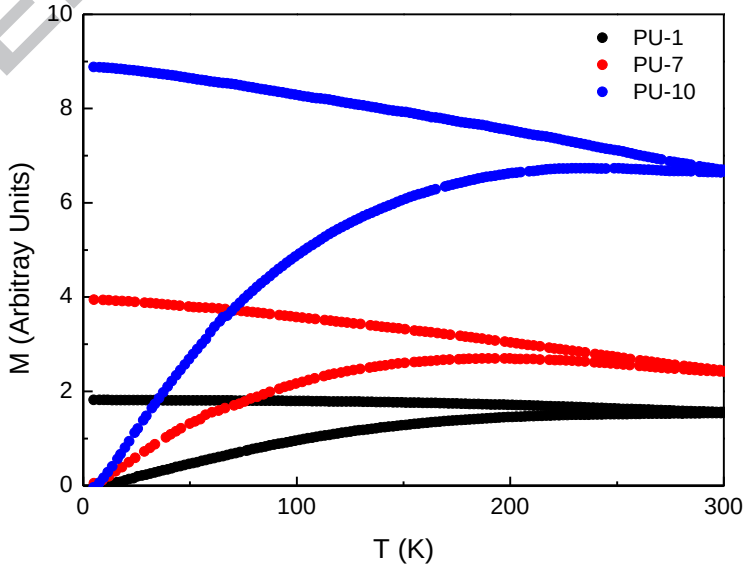

Figure 2. ZFC/FC curves for nanocomposite samples containing 1, 7 and 10 nominal wt.% MNP measured with an applied field of 4kA/m.

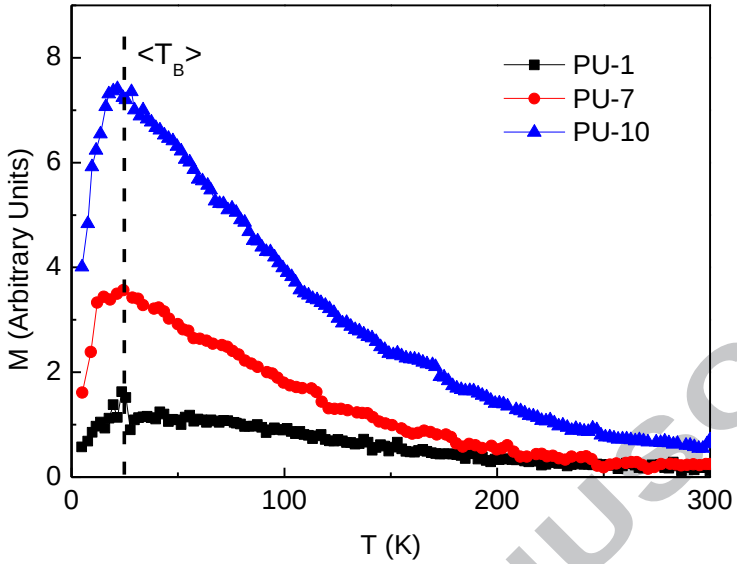

Figure 3: M_{ZFC}- M_{FC} versus temperature curves for nanocomposite samples containing 1, 7 and 10 nominal wt.% MNP measured with an applied field of 4 kA/m.

Table 1: Mean blocking temperatures (<T_B>), sample magnetization (M) at high field and coercive field (Hc) at 5 K for nanocomposite samples containing 1, 7 and 10 nominal wt.% MNP.

Sample	**<T_B> (K)**	**M (emu/g sample) (H=20 kOe), 300 K**	**M (emu/g sample) (H=20 kOe), 5 K**	**Hc (Oe) 5 K**
PU-1	26.6 ± 0.5	0.13 ± 0.01	0.15 ± 0.01	295 ± 16
PU-7	24.3 ± 0.5	2.86 ± 0.01	3.24 ± 0.10	304 ± 2
PU-10	21.6 ± 0.5	4.90 ± 0.20	5.50 ± 0.10	328 ± 4

Figures 4 a-c show magnetic field dependence magnetization at two different temperatures (5 K and 300 K), for the PUs with 1, 7 and 10 wt.% MNP. A magnification of the central area of the magnetization loops is shown in the inset, to give a better idea of the coercive field behavior. The values of coercive field (Hc) at 5 K, as well as the magnetization (M) values at high field (±20 kOe) for the composite samples containing 1, 7 and 10 wt.% MNP are also summarized in Table 1. As the content of nanoparticles increases, M also increases due to the increased amount of

magnetic material in the sample. However, none of the samples reaches saturation magnetization (i.e. dM/dH ≠ 0 at ±20 kOe) in the conditions selected for the tests. The magnetization at high field (±20 kOe) values decreases as the temperature increases, which is consistent with the super-paramagnetic regime at 300 K in comparison with the blocked state at 5 K. As reported in a previous paper, the actual content of magnetic particles in the composite samples was determined from thermogravimetric analysis (TGA) and resulted lower than the nominal one ([4], data also included in Table 3). Thus, using this information the nanoparticles magnetization was calculated as 77.4 emu/g magnetic particles for the PU-10 sample, which compares very well with the saturation magnetization of spherical magnetite nanoparticles (i.e. 77.5 emu/g for nanomagnetite with average diameter of 11.5 nm at 5 K, ref. [20]). Considering that the nanoparticles used in all the samples come from the same batch, the nanoparticles' magnetization should be the same if it is calculated from a different sample. However, we obtained minor differences in M (expressed in emu per Fe-oxide grams) when it was calculated from samples PU-1 and PU-7, which were attributed to the error of the weighing machine used to determine the involved masses.

The super-paramagnetic behavior at room temperature can be corroborated by the absence of hysteresis at 300 K (i.e. zero value of coercive field), together with the ZFC/FC measurements as indicated previously. At temperatures below T_B, the magnetic particles are in the blocked regime, and the magnetic relaxation time at that temperature is greater than the measurement time and consequently, hysteresis appears in the magnetization curve, as can be seen on magnetization loops measured at 5 K. From coercive fields at 5 K, non-significant difference between the different samples was found. Finally, to confirm the similar magnetic behavior of the tree samples (PU-1, PU-7 and PU-10) normalized field dependence magnetization were plotted together, as shown in Figure 4d. As can be noticed, almost no differences between the samples are observed.

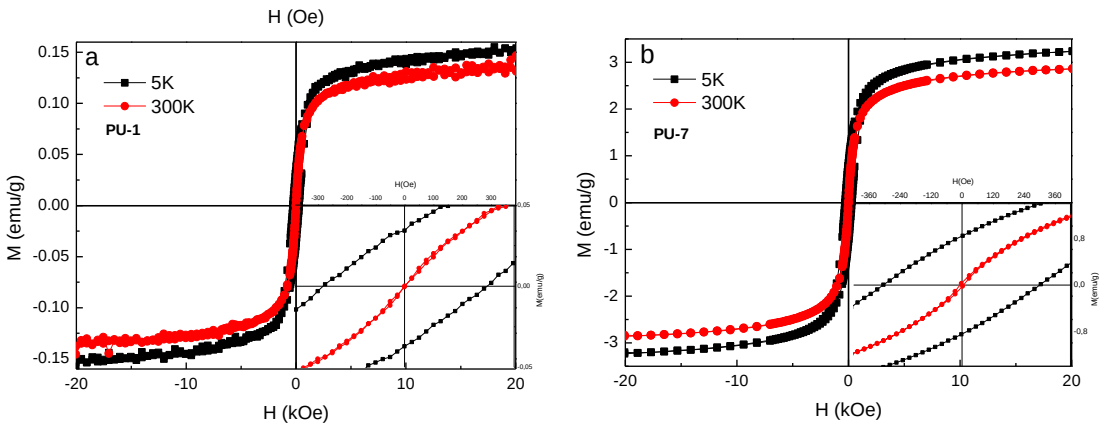

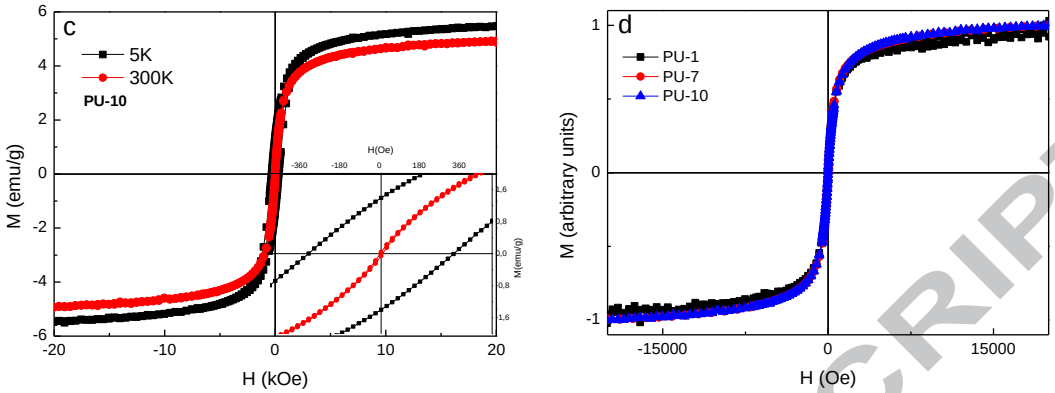

Figure 4: a-c) Magnetization vs. applied field curves at 5 and 300 K for nanocomposite samples containing 1, 7 and 10 nominal wt.% MNP. **d)** Normalized magnetization vs. applied field curves at 300 K for nanocomposite samples containing 1, 7 and 10 nominal wt.% MNP.

SAXS measurements were carried out on all samples at 20 and 60 °C, to study the behavior of the composites below and above the melting temperature of the PU soft segments, which changes from 38.8 to 36.7 °C as the MNP content increases from 0 to 10 nominal wt.% [4]. SAXS curves for nanocomposite films at 20 °C presented as log (I(q)) versus log (q) are shown in Figure 5. Curves obtained at 60 °C are similar to those presented in Figure 5 and thus are not included. Guinier and Porod regions were analyzed to obtain structural information and arrangement features of the nanoparticles loaded within the matrices.

At the low-q region, the scattering intensity I(q) produced by an isotropic and dilute set of isolated particles embedded in a homogeneous matrix can be described by the Guinier law [21]:

$$I(q) = G\exp(-q^2 R_g^2/3) \quad (2)$$

where q is the momentum transfer vector, I(q) is the scattering intensity that depends on q, G is the Guinier pre-factor and Rg the radius of gyration of the particles. Thus, for spherical particles of diameter D [22], Rg is given by:

$$R_g = \left(\frac{3}{5}\right)^{0.5} \frac{D}{2}. \quad (3)$$

Using Eq. 2 and Eq. 3, values of D ranging between 25.5 and 27 nm were determined for SAXS patterns obtained at 20 ºC, while for the measurements performed at 60 ºC, D values oscillate between 22.7 and 25.3 nm, as presented in Table 2. As can be noted, all

the values are larger than those obtained from TEM for single nanoparticles. This fact can be indicating that single nanoparticles are forming compact scattering entities (clusters) within the matrices. In addition, the particle diameters estimated from samples that have their polyurethane soft segments melted (60 °C) are lower than those calculated at 20°C, which could be an indication about that the particles were preferably located in the soft domains of the polymeric matrix. Notice also that the diameter of the scattering objects (clusters) in all the samples fall into a narrow range, which point out that the cluster size is independent of the nanoparticle concentration. However, a decrease in the cluster-cluster distance is expected as the nanoparticle concentration increases.

For an ideal two-phase system with a well defined interface, Porod's law predicts that I(q) decreases as q^{-4} for large q, where the value of −4 for the slope (α) represents the 2D surface of a smooth object [23-27]. Other values of α have been interpreted using fractal geometry [24]. Thus, if $3 \leq |\alpha| < 4$ then $6-|\alpha|$ is the surface fractal dimension, Ds ($2 < Ds \leq 3$). When $1 \leq |\alpha| < 3$, then the value of $|\alpha|$ is a mass fractal dimension, $Dm = |\alpha|$. In the present case and for all the samples and temperatures, the intensity follows a power-law with q in the Porod's region (0.7-1 nm^{-1}) with the exponent varying between -3.93 and -3.08, corresponding to fractal dimension Ds in the range of 2.07–2.92. These values are also listed in Table 2. The slopes in the Porod's region fell in the range of -4 to -3, implying rough particle surfaces [28]. The fractal dimension is lower for the most concentrates samples, indicating a rather smooth surface, which could be related with low amount of polymeric matrix adhered on their surfaces due to the reduced compatibility between nanoparticles and polymeric matrix, as was envisaged in our previous work [4]. On the other hand Ds is closer to 3 for PU-1, indicating a surface that fills the space almost completely [29].

Table 2: Particle diameter (D), power law of scattering (α) and surface fractal dimension (Ds) calculated from SAXS curves.

MNP nominal wt. %	20 °C			60 °C		
	D (nm)	α	Ds	D (nm)	α	Ds
1	27.0	-3.47	2.53	25.3	-3.08	2.92
3	26.1	-3.90	2.10	23.0	-3.86	2.14
5	25.8	-3.88	2.12	23.2	-3.93	2.07
7	25.5	-3.83	2.17	22.7	-3.80	2.20
10	25.8	-3.86	2.14	22.8	-3.81	2.19

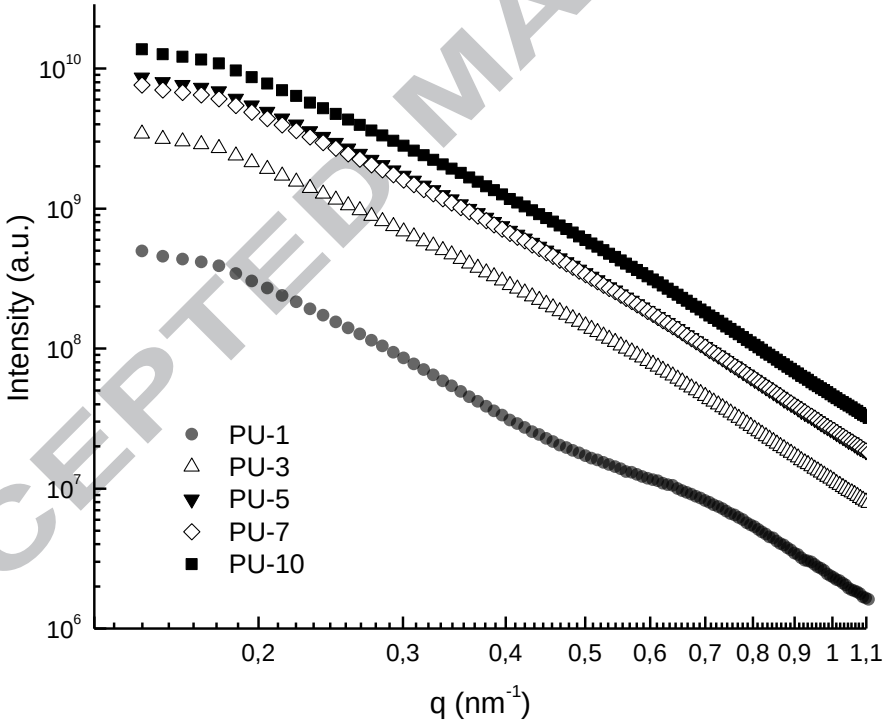

Figure 5: Small angle X-ray scattering intensity (I) as a function of the momentum transfer vector (q) for nanocomposite films, obtained at 20 °C.

For illustrative purposes, a set of composite samples, initially at room temperature, was submitted to magnetic heating by applying an alternant magnetic field (143 kHz). Since the samples were located in different positions inside the coil, the AC field they

received was slightly different: 18.9 ± 6 kA/m for the samples located at the corner or 17.8 ± 2 kA/m for the other samples). The thermographic images of the set of samples taken at different heating times are shown in Figure 6. It is clear that both, the final temperature reached for the sample as well as the heating rate strongly depend on the MNP content. It is also clearly noticed that the changes in the temperature of the neat matrix (PU-0) and less concentrated composite (PU-1) are negligible. To quantify the heating rate, records of sample temperature vs. time during the application of a magnetic field were obtained for each sample by an optic fiber sensor. For this, each sample was placed in the middle of the coil and exposed to an alternant magnetic field of 48.5 kA/m and 260 kHz. Three consecutive heating runs per sample were performed. In Figure 7a the results for sample PU-7 sample are shown. As can be noted, the first run presents a different slope between 35 ºC and 40 ºC, which is related to the melting of the soft segments of the polyurethane matrix [4], as discussed in the next section. The heating rate of composite samples obtained as the mean slope of the second a third heating runs is presented in Figure 7b. Three different zones can be noticed in the figure: the heating rate of the most diluted sample is low; the heating rates of the samples containing intermediate contents of MNP is also intermediate and follows a linear dependence with filler concentration, and the heating rate of the most concentrated sample almost double the value of the previous samples, which could be related with the magnetic percolation threshold for the MNP into the PU matrix.

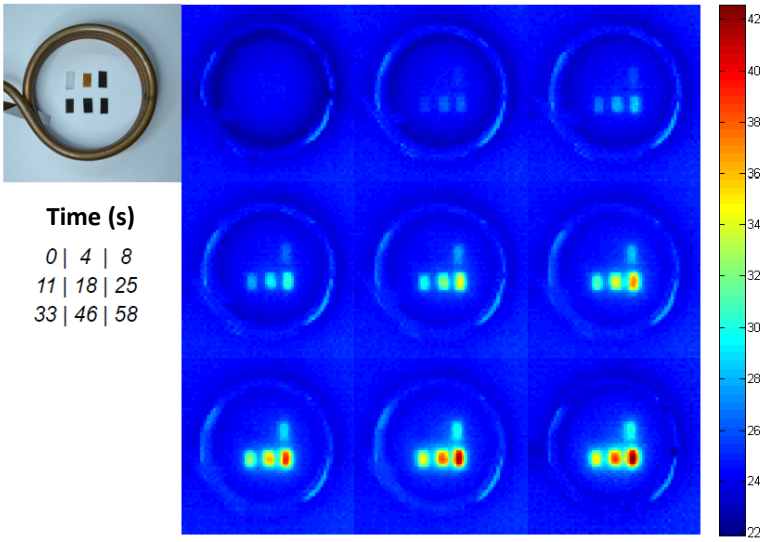

Figure 6: Temperature maps for nanocomposite pieces of 4.9 mm × 10.9 mm length as a function of the time of application of an alternant magnetic field of 143 kHz and 18.9 ± 6 kA/m (samples located at the corner) or 17.8 ± 2 kA/m (other samples). From top left to right bottom: PU-0, PU-1; PU-3; PU-5; PU-7 and PU-10.

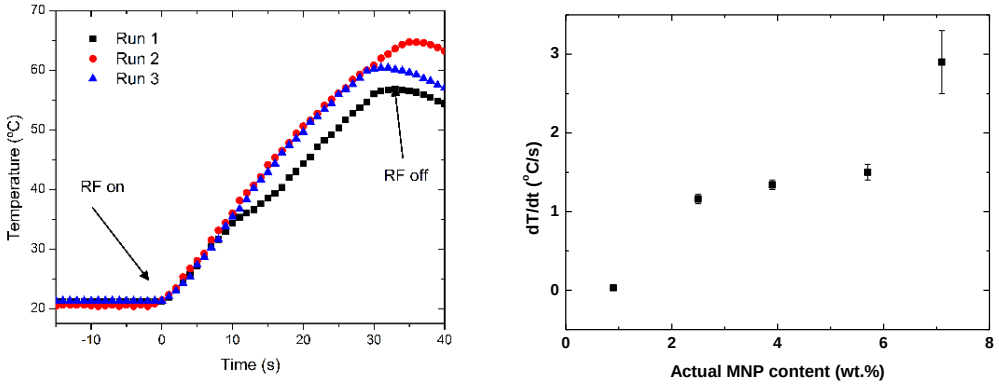

Figure 7: a) Temperature versus time measurement for sample PU-7. The times at which the alternant magnetic field (RF) is turn on and turn off are indicated. Three consecutive heating runs are shown; b) Heating rate of nanocomposite samples submitted to magnetic heating.

To determine the specific absorption rate, the heat capacity of the composites was measured as a function of the temperature, as shown in Figure 8. It is noticed that the heat capacity of the samples decreases as MNPs concentration increases, as was also reported in related papers [30, 31]. Moreover, around 40ºC, there is a fluctuation in the functionality of the heat capacity with the temperature, which is due to the melting of

the soft segments of the polyurethane matrix [4]. Also, the obtained values differ slightly if they are evaluated from the first or the second heating runs, due to the crystallization of these segments, that took place during relatively long time (aged samples, fist run) or relatively quickly (samples with erased thermal history that crystallize during cooling, second run). The functionality of the heat capacity with the temperature also seems to depend on the MNP content, although this dependence is strong at temperatures higher than the equilibrium one (~25°C), which is the temperature reached by the neat matrix (PU-0) after the application of the alternant magnetic field. All these observations could be related with the complexity of the composites that combine a segmented polyurethane matrix, involving four thermal transitions (two glass transition temperatures added to two melting events) with magnetic nanoparticles. Thus, the averaged values between the first and second runs for each composite were selected for the calculation of the SAR values. These results are presented in Table 3. Independently of the unit of mass used to calculate SAR values (nominal or actual particle content), it is clear that SAR increases very much from sample PU-1 to PU-3 and then it is reduced by half and remains approximately constant for concentrations greater than 3% MNP. The opposite behaviors showed by the heating rate and the heat capacity with MNP concentration compensate themselves, leading to SAR values that do not change very much with MNP concentration when the 3 nominal wt.% is exceeded. The specific absorption rate, often denominated as heating efficiency, is directly related to the heat losses of the MNPs when exposed to the AC field, and it is given by the hysteresis loop area of the MNPs [32]. Therefore, the SAR should be improved by increasing the area of the AC hysteresis loop, which is essentially proportional to the saturation magnetization (Ms) and the coercive field (Hc) of the MNPs. For our composite films it is noticed that the M values at 20 kOe, which are proportional to Ms values, increase as the MNP concentration increases since the contribution of the paramagnetic matrix decreases. In the same way the Hc values increase slightly with MNP concentration. Thus, we believe that the maximum observed in the PU-3 sample is due to the relative contribution of those different sources that present differing behavior with MNP concentration. Regarding SAR absolute values, it is known that the structure and chemical composition of magnetic nanoparticles, their coating and the viscosity of the suspending medium have a tremendous effect on the heat producing efficiency [33]. The latter parameters control the ratio of Brownian and Néel mechanisms in the process of magnetic relaxation and thus by their optimization

the SAR values can be maximized for a given nanoparticle dispersion. In this line, it should be empathized that most of the SAR values found for nanomagnetite containing systems were obtained from water/organic solvents diluted dispersions, not from solid films like ours. For example, Liang et al [34] investigated the specific absorption rate of Fe_3O_4 nanoparticles with different sizes (i.e. 4 nm, 20 nm, 50 nm and 200 nm) prepared by a rapid microwave synthetic strategy. SAR values (alternant magnetic field, 390 and 780 kHz, 12 A) obtained ranged from 33.6 W/g for 4 nm particles at 390 kHz to 1457.2 W/g for 20 nm particles at 780 kHz, which surprised the authors since the observed enhanced heating capacity for the 20 and 50 nm particles was not consistent with the saturation magnetization that increases as particle size increases (from 42 to 95 emu/g for 4 to 200 nm particle). Moreover, they attributed the high SAR values for 20 and 50 nm Fe_3O_4 nanoparticles to comprehensive contributions from Brownian losses (friction arising from total particle oscillations), Neél losses (rotation of the magnetic moment with each field oscillation) and single domain particle hysteresis effect [32, 34]. In these aspects, the size of the particles embedded in our films, as calculated by SAXS measurements (Table 2), is well in the range of those that give the enhanced SAR. However, it is not correct to equal cluster size to effective magnetic size, especially for small super-paramagnetic nanoparticles embedded in a matrix. In fact, the magnetic response as obtained from hyperthermia measurements is going to correspond to that of the individual nanoparticles (5-12 nm), not to the cluster (unless interactions are considered). Nevertheless, even when our particle sizes could be far from the optimum sizes for enhancing the heating efficiency and also taking into account that the dispersion in shapes and sizes is also going to limit the heating efficiency of our samples, a very fast recovery of the original shape was achieved, as is discussed in the next section. In addition, is interesting to mention that Thorat and coworkers [35] achieved SAR values at the level of 400 W/g, for iron oxide nanoparticles at high magnetic field strengths (~40 kA/m) by designing specific polymer coatings. On the other hand, Illés et al [33] prepared biocompatible magnetite nanoparticles (MNPs) based on magnetite by post-coating the magnetic nanocores with a synthetic polymer designed specifically to shield the particles from non-specific interaction with cells. The SAR values obtained for these particles were 50.3 W/g at 323 kHz/15.9 kA/m when it was measured in a DM100 device but only 17.44 W/g at 329 kHz/13.13 kA/m when it was obtained from a magneTherm instrument. These values also highlight the strong

discrepancy between the SAR values obtained for same materials in different experiments, as reported in related papers [36, 37].

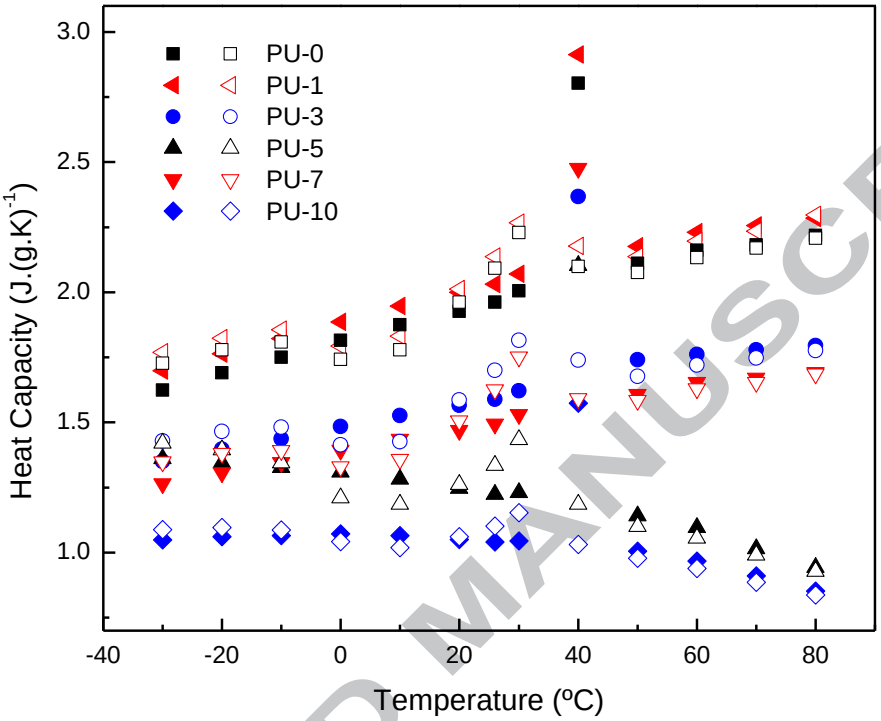

Figure 8: Heat capacity at constant pressure [J.(g.K)$^{-1}$] of PU composites and neat matrix as a function of temperature. Filled symbols correspond to the determination of heat capacity from 1st heating and unfilled symbols to the 2nd heating.

Table 3: Average heat capacity and SAR values (magnetic field applied = 48.5 kA/m and 260 kHz) for nanocomposite samples.

MNP Nominal wt. %	**MNP Actual wt. %**	**Cp (J (kg K)$^{-1}$)**	**SAR (W (g)$^{-1}$) nominal MNP content**	**SAR (W (g)$^{-1}$) actual NMP content**
1	0.9 ± 0.1	2084 ± 74	6.5	7.2
3	2.5 ± 0.2	1644 ± 78	63.6	76.3
5	3.9 ± 0.8	1279 ± 78	34.3	44.0
7	5.7 ± 1.4	1560 ± 92	33.4	41.0
10	7.1 ± 0.1	1071 ± 43	31.0	43.7

Finally, the shape memory response of the composites to an external magnetic field was qualitatively evaluated. Figure 9a shows selected images of the heating experiments by the application of a radiofrequency field (260 kHz, 48.5kA/m) on samples containing 1, 7 and 10 nominal wt.% MNP. A fast and almost complete recovery of the original shape of the nanocomposites containing more than 1 nominal wt.% MNP (PU-3, PU-5, PU-7 and PU-10) was reached in less than 35 seconds, with decreasing recovery time as nanoparticle concentration in the composite increases. However, more than 2 minutes were necessary to almost recover the original shape of the PU-1 sample, even when its initial deformation was lower than those imposed to the concentrated samples. The neat matrix, on the other hand, did not show any response to the applied field even when it was kept for more than 5 minutes. To correlate the recovery of the original shape process with the sample's temperature, thermographic images were taken at different times during the experiment. In Figure 9b some representative images corresponding to sample PU-10 (16.8 mm x 5.26 mm x 0.82 mm) are shown. The sample begins to recovery its original shape at 34ºC and the process is complete at 50 ºC.

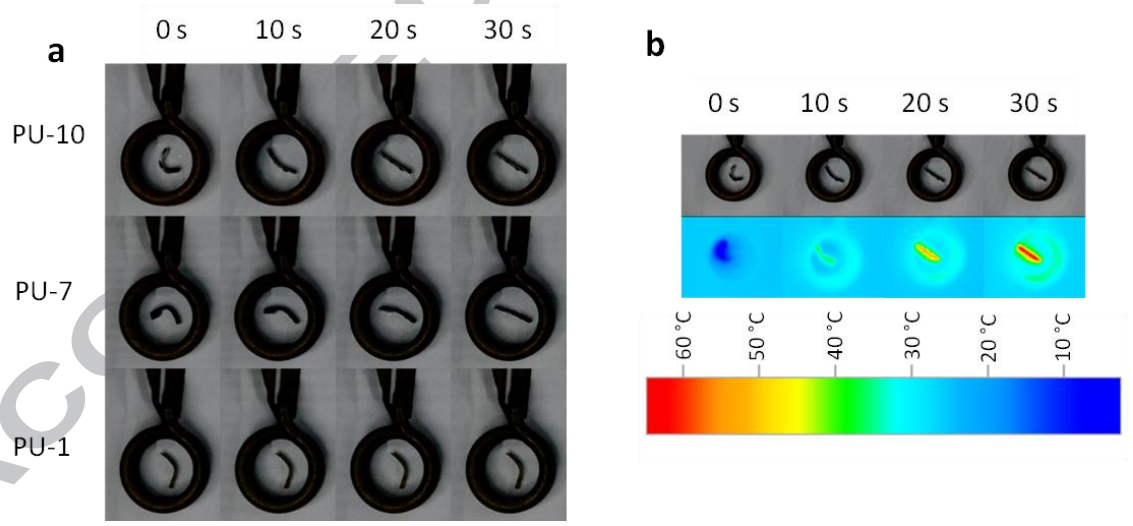

Figure 9: a) Shape recovery of samples containing 0, 1, 7 and 10 nominal wt.% MNPs activated by the application of an alternant magnetic field; b) Shape recovery of sample PU-10 activated by the application of an alternant magnetic field, registered simultaneously with an optic camera and a thermographic one.

CONCLUSIONS

Magnetic nanocomposites with shape memory, prepared by a simple casting procedure, were characterized in terms of magnetic response and inductive heating. The size of the synthesized magnetic particles was estimated by TEM while the size of the clusters included in the polyurethane matrix was obtained from SAXS calculations. Even when some particle agglomeration in the polymeric matrix was found, the composites exhibited super-paramagnetic behavior and interesting specific absorption rates even for concentrations as low as 1 nominal wt.% MNP. What is more, a fast and almost complete recovery of the original shape of the nanocomposites containing more than 3 nominal wt.% MNP was obtained by application of an alternant magnetic field to the previously deformed samples. We believe that this study will certainly help to define potential technological applications for the developed nanocomposites.

ACKNOWLEDGEMENTS

The authors acknowledge the financial support provided by the Science and Technology National Promotion Agency (ANPCyT, Grant PICT-2013-1535), CONICET (Grant No. PIP 11220110100720CO), UNLP (Grant No. 11/X680) and the National University of Mar del Plata (Project # 15/G494), all of them from Argentina. We also thank Bunge y Born Foundation for the fellowship awarded to Dr. Guillermo Soto. Dr. Diego Muraca acknowledge the Brazilian Nanotechnology National Laboratory (LNNano) for the use of electron microscopy facility under the project ME–22345, Brazilian agencies Fundação de Amparo à Pesquisa do Estado de São Paulo (FAPESP Project # 2011-12356) and National Council for Scientific and Technological Development (CNPq Project # 303236/2017-5)

DATA AVAILABILITY

The raw/processed data required to reproduce these findings cannot be shared at this time as the data also forms part of an ongoing study.

REFERENCES

1. Abbasi, A., G. Mir Mohamad Sadeghi, and I. Ghasemi, *Synthesis and characterization of novel environmentally friendly shape memory polyurethanes based on poly(epsilon-caprolactone) diol/castor oil mixtures.* Polymer Science, Series B, 2017. **59**(5): p. 526-536.

2. Shu- Ying, G., C. Kun, and J. Sheng- Peng, *A dual- induced self- expandable stent based on biodegradable shape memory polyurethane nanocomposites (PCLAU/Fe3O4) triggered around body temperature.* Journal of Applied Polymer Science, 2018. **135**(3): p. 45686.
3. Urban, M. and M. Strankowski, *Shape Memory Polyurethane Materials Containing Ferromagnetic Iron Oxide and Graphene Nanoplatelets.* Materials, 2017. **10**(9): p. 1083.
4. Soto, G.D., et al., *Nanocomposites with shape memory behavior based on a segmented polyurethane and magnetic nanostructures.* Polymer Testing, 2018. **65**: p. 360-368.
5. Hua, Z., W. Christoph, and S.Y. C., *Shape- Memory Polyurethane Nanocomposites with Single Layer or Bilayer Oleic Acid- Coated Fe3O4 Nanoparticles.* Macromolecular Materials and Engineering, 2015. **300**(9): p. 885-892.
6. Aida, A., et al., *Shape memory performance of green in situ polymerized nanocomposites based on polyurethane/graphene nanoplatelets: Synthesis, properties, and cell behavior.* Polymer Composites. **0**(0).
7. Peponi, L., et al., *Synthesis and characterization of PCL–PLLA polyurethane with shape memory behavior.* European Polymer Journal, 2013. **49**(4): p. 893-903.
8. Xiao, L., et al., *Water-soluble superparamagnetic magnetite nanoparticles with biocompatible coating for enhanced magnetic resonance imaging.* ACS Nano, 2011. **5**(8): p. 6315-6324.
9. Wu, J.H., et al., *Sub 5 nm magnetite nanoparticles: Synthesis, microstructure, and magnetic properties.* Materials Letters, 2007. **61**(14-15): p. 3124-3129.
10. Sun, S. and H. Zeng, *Size-controlled synthesis of magnetite nanoparticles.* Journal of the American Chemical Society, 2002. **124**(28): p. 8204-8205.
11. Kloster, G.A., N.E. Marcovich, and M.A. Mosiewicki, *Composite films based on chitosan and nanomagnetite.* European Polymer Journal, 2015. **66**: p. 386-396.
12. Lu, A.H., E.L. Salabas, and F. Schüth, *Magnetic nanoparticles: Synthesis, protection, functionalization, and application.* Angewandte Chemie - International Edition, 2007. **46**(8): p. 1222-1244.
13. Mohr, R., et al., *Initiation of shape-memory effect by inductive heating of magnetic nanoparticles in thermoplastic polymers.* Proceedings of the National Academy of Sciences of the United States of America, 2006. **103**(10): p. 3540-3545.
14. Rosensweig, R.E., *Heating magnetic fluid with alternating magnetic field.* Journal of magnetism and magnetic materials, 2002. **252**: p. 370-374.
15. Brown, W., *Thermal fluctuation of fine ferromagnetic particles.* IEEE Transactions on Magnetics, 1979. **15**(5): p. 1196-1208.
16. Dormann, J.L., D. Fiorani, and E. Tronc, *On the models for interparticle interactions in nanoparticle assemblies: comparison with experimental results.* Journal of Magnetism and Magnetic Materials, 1999. **202**(1): p. 251-267.
17. Thanh, N.T., *Magnetic Nanoparticles: From Fabrication to Clinical Applications*. 2012, Didcot, UK: Taylor & Francis Group.
18. Yu, W.C., S.; Lim, T.-C.; U. Rajendra Acharya, ed. *Advances in Therapeutic Engineering*. 2013, Taylor & Francis Group: Didcot, UK.

19. Bezdorozhev, O., T. Kolodiazhnyi, and O. Vasylkiv, *Precipitation synthesis and magnetic properties of self-assembled magnetite-chitosan nanostructures.* Journal of Magnetism and Magnetic Materials, 2017. **428**: p. 406-411.
20. Goya, G.F., et al., *Static and dynamic magnetic properties of spherical magnetite nanoparticles.* Journal of Applied Physics, 2003. **94**(5): p. 3520-3528.
21. Silva, N., et al., *Structure of magnetic poly (oxyethylene)–siloxane nanohybrids doped with FeII and FeIII.* Journal of applied crystallography, 2003. **36**(4): p. 961-966.
22. Petrović, Z.S., et al., *Effect of silica nanoparticles on morphology of segmented polyurethanes.* Polymer, 2004. **45**(12): p. 4285-4295.
23. De Oliveira Patricio, P.S., et al., *Tailoring the morphology and properties of waterborne polyurethanes by the procedure of cellulose nanocrystal incorporation.* European Polymer Journal, 2013. **49**(12): p. 3761-3769.
24. Peyronel, F., et al., *Ultra small angle x-ray scattering in complex mixtures of triacylglycerols.* Journal of Physics Condensed Matter, 2014. **26**(46).
25. Bisoi, A.K. and J. Mishra, *On calculation of fractal dimension of images.* Pattern Recognition Letters, 2001. **22**(6-7): p. 631-637.
26. Foroutan-pour, K., P. Dutilleul, and D.L. Smith, *Advances in the implementation of the box-counting method of fractal dimension estimation.* Applied Mathematics and Computation, 1999. **105**(2-3): p. 195-210.
27. Mandelbrot, B.B., *The fractal geometry of nature.* Science, 1967. **155**(6): p. 636-638.
28. Duan, Y., et al., *Self-crosslinkable poly(urethane urea)-reinforced silica aerogels.* RSC Advances, 2015. **5**(88): p. 71551-71558.
29. Laaksonen, A., et al., *Surface fractal dimension, water adsorption efficiency, and cloud nucleation activity of insoluble aerosol.* Scientific Reports, 2016. **6**: p. 25504.
30. Razzaq, M.Y., et al., *Thermal, electrical and magnetic studies of magnetite filled polyurethane shape memory polymers.* Materials Science and Engineering A, 2007. **444**(1-2): p. 227-235.
31. Weidenfeller, B. and M. Anhalt, *Polyurethane-magnetite composite shape-memory polymer: Thermal properties.* Journal of Thermoplastic Composite Materials, 2014. **27**(7): p. 895-908.
32. Nemati, Z., et al., *Enhanced Magnetic Hyperthermia in Iron Oxide Nano-Octopods: Size and Anisotropy Effects.* Journal of Physical Chemistry C, 2016. **120**(15): p. 8370-8379.
33. Illés, E., et al., *Multifunctional PEG-carboxylate copolymer coated superparamagnetic iron oxide nanoparticles for biomedical application.* Journal of Magnetism and Magnetic Materials, 2018. **451**: p. 710-720.
34. Liang, Y.-J., et al., *Size-dependent electromagnetic properties and the related simulations of Fe3O4 nanoparticles made by microwave-assisted thermal decomposition.* Colloids and Surfaces A: Physicochemical and Engineering Aspects, 2017. **530**: p. 191-199.
35. Thorat, N.D., et al., *Superparamagnetic iron oxide nanocargoes for combined cancer thermotherapy and MRI applications.* Physical Chemistry Chemical Physics, 2016. **18**(31): p. 21331-21339.
36. Périgo, E.A., et al., *Fundamentals and advances in magnetic hyperthermia.* Applied Physics Reviews, 2015. **2**(4).

37. Etheridge, M., et al., *Superparamagnetic iron oxide nanoparticle heating: A basic tutorial.* Nanoparticle heat transfer and fluid flow, 2012: p. 97-121.

Graphical abstract

MAGNETIC NANOCOMPOSITES BASED ON SHAPE MEMORY POLYURETHANES

G. D. Soto, C. Meiorin, D. Actis, P. Mendoza Zélis, Oscar Moscoso Londoño, Diego Muraca, M. A. Mosiewicki, N. E. Marcovich

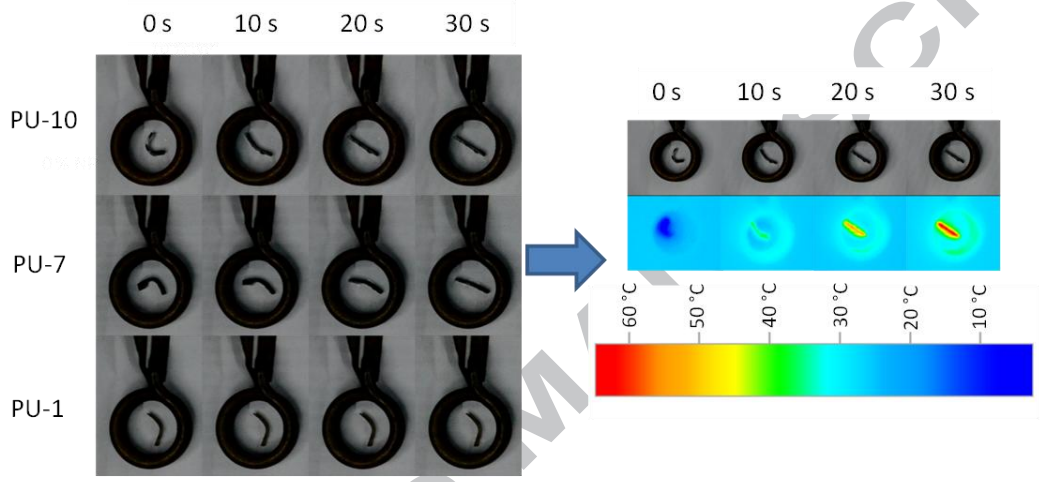

Highlights

- Magnetic nanocomposites with shape memory properties are prepared by a simple casting procedure.
- Nanocomposites present super-paramagnetic behavior with mean blocking temperatures between 21 and 27 K.
- Nanocomposites' temperature increases when they are exposed to an alternant magnetic field.
- Nanocomposites' original shape is recovered by applying magnetic heating as indirect triggering method.
- A fast and almost complete recovery of the original shape of the samples containing more than 3 nominal wt.% MNP is obtained.